Available online at www.sciencedirect.com

ScienceDirect

Procedia CIRP 00 (2018) 000–000

www.elsevier.com/locate/procedia

4th CIRP Conference on Surface Integrity (CSI 2018)

Large strain extrusion machining of magnesium alloys for biomedical applications

R. Bertolini[a]*, S. Bruschi[a], A. Ghiotti[a], L. Pezzato[a], M. Dabalà[a]

[a]*Dept. of Industrial Engineering, University of Padova, Via Venezia 1, 35131, Padova, Italy*

* Corresponding author. Tel.: +39-049-827-6819; fax: +39-049-827-6819. *E-mail address:* rachele.bertolini@dii.unipd.it

Abstract

Recently, magnesium alloys are attracting more and more attention as degradable materials for manufacturing temporary biomedical devices, although their rapid degradation in physiological environment limits their clinical applications to a great extent. Different Severe Plastic Deformation (SPD) processes have been recently applied to magnesium alloys in order to improve the surface integrity, which is directly correlated to their corrosion resistance. The current study investigates the possibility of exploiting Large Strain Extrusion Machining (LSEM) as a processing route to increase corrosion resistance of magnesium alloys for biomedical applications. Different cooling conditions and cutting speeds were adopted during LSEM and their effects on the surface integrity and corrosion resistance on both the machined workpiece and obtained chips were studied. For the first time, liquid nitrogen was used as cooling medium in LSEM and its effect was properly investigated. Results showed that LSEM, regardless of the adopted cutting parameters, is an effective method to obtain a workpiece with improved functional performances. Similar results pertain to the chips, but a careful choice of process parameters is even more mandatory than in the case of the workpiece.

Peer-review under responsibility of the scientific committee of the 4th CIRP Conference on Surface Integrity (CSI 2018).

Keywords: Large strain extrusion machining; cryogenic cooling; surface integrity; corrosion resistance

1. Introduction

Magnesium alloys are emerging as potential candidates for producing degradable temporary implants, since they have the ability to dissolve in human environment and remain non-toxic thanks to their high biocompatibility [1]. However, their reduced corrosion resistance to human body fluids leads to the loss of mechanical stability of the implant before the bone complete healing, thus limiting their actual applicability in the biomedical field.

Intense grain refinement pursued by Severe Plastic Deformation (SPD) is one of the main strategies used by researchers to increase corrosion resistance of magnesium alloys [2]. In the past decade, different SPD approaches, such as Equal Channel Angular Extrusion (ECAE) [3], roller burnishing [4], and High-Pressure Torsion (HPT) [5] have been applied to obtain grain refinement on bulk magnesium alloys. Studies in [6,7,8] demonstrated that Large Strain Extrusion Machining (LSEM) can be also classified as a SPD process combining, in a single step, large strains induced by machining both in the machined workpiece and chips with the chip dimensional control thanks to extrusion.

In this work, LSEM is applied to machining of the AZ61 magnesium alloy with the aim of proving that the obtainable severe deformation of both the workpiece and the chips can help in increasing the AZ61 corrosion resistance in human-like environment. Furthermore, liquid nitrogen as cooling medium is here used for the first time, as it was proved to further increase the machined surface deformation and resistance [9], besides being non-toxic and therefore suitable for machining biomedical components.

Different cutting speeds and cooling strategies were applied during LSEM of AZ61 and their effects on the surface integrity and corrosion behavior of both the machined workpiece and the LSEM-ed chips were investigated. Results show that cryogenic cooling can be efficiently applied to the LSEM process to

Peer-review under responsibility of the scientific committee of the 4th CIRP Conference on Surface Integrity (CSI 2018).

obtain a workpiece with enhanced corrosion properties in human-like environment. Conversely, much more effort is needed to make the obtained chips usable as sheet components, since the application of liquid nitrogen limits the chip formability.

Nomenclature

LSEM	large strain extrusion machining
to	undeformed chip thickness
tc	controlled chip thickness
tw	width of cut
Vo	cutting speed
Vc	chip speed
α	rake angle
λ	chip compression ratio
γ	shear strain

2. Mechanics of LSEM

LSEM is a single-step plane strain deformation process that combines large shear strains induced by machining with proper dimensional control of the extruded chips. The obtained chips are in form of sheet produced directly from the bulk material in a single stage of deformation. Fig. 1 reports a scheme of the process.

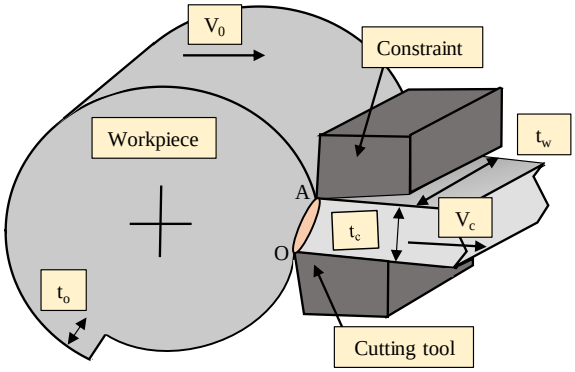

Figure 1. Scheme of the LSEM process.

A constraining tool is placed above the cutting tool, which travels at cutting speed V_0, with the aim of extruding the chip from t_0 to t_c. The chips are formed by shear in a narrow deformation zone idealized as the shear plane OA in Fig. 1. The chip speed can be calculated as $Vc = Vo/tc$.

An estimation of the shear strain γ at the shear plane is given by the following formula (1), according to [10]:

$$\gamma = \frac{\lambda}{\cos(\alpha)} + \frac{1}{\lambda * \cos(\alpha)} - 2\tan(\alpha) \quad (1)$$

where α is tool rake angle and λ the chip compression ratio, namely the ratio between t_c an t_0. A wide range of shear strains can be obtained by an appropriate selection of α and λ.

3. Experimental

3.1. Material under investigation

The material objective of the study was the commercially available AZ61 magnesium alloy supplied in form of bars of 60 mm of diameter and 500 mm of length. The bars were subjected to an annealing treatment at 360°C for 2 hours, which led to a homogenous average grain size of 15 μm.

3.2. LSEM experimental set-up

The LSEM tests were carried out on a Mori Seiki™ lathe, equipped with a specially designed apparatus that included the constraint tool, placed above the cutting tool to fulfill large strain extrusion cutting conditions, and the liquid nitrogen supply system. More details about the system for liquid nitrogen delivery and storage can be found in [11]. The adopted cutting tool was a Sandvik Coromant™ semi-finishing insert VBMW160404H13A, with rake and clearance angles of 0° and 5°, respectively.

The imposed undeformed chip thickness *to* was 0.2 mm, while the chip compression ratio λ was set equal to 1.25. The constraint tool corner radius was set equal to 0.4 mm in order to maximize the effective strain that could be produced on the workpiece, according to [12]. Since the main aim of the study was to investigate the effect of cryogenic cooling applied to LSEM, λ was kept fixed for all the tests. Different cutting speeds, namely 30 m/min, 60 m/min and 120 m/min, and different cooling conditions, namely dry cutting and cryogenic cooling, were applied. A standard cutting fluid was also initially used, however the machine tool system sprayed it at too high pressure, without any chance of modification, leading to the formation of discontinuous, thus not suitable, chips. The LSEM experiments were repeated three times in order to assure repeatability of the obtained results.

Table 1. Experimental plan for the LSEM tests.

Test ID	Cutting speed (m/min)	Cooling condition
D1	30	Dry
D2	60	Dry
D3	120	Dry
C1	30	Cryogenic
C2	60	Cryogenic
C3	120	Cryogenic

3.3. Microstructural and mechanical characterization

First, a macroscopic analysis of the chips morphology was carried out using a Leica DMRE™ optical microscope equipped with a high definition digital camera with a magnification of 50X. Later on, both the machined cylinders and LSEM-ed chips were cut to prepare metallographic samples. After cold mounting, grinding and polishing, the samples were etched with an acetic and picric acid aqueous solution to reveal the grain boundaries and then inspected with the microscope.

The extent of the machining-affected layer of the machined bar was evaluated on the basis of the following procedure: the layer thickness was measured from optical microscope images recorded at 500X magnification every 30 μm, the measures were repeated in two different zones of the sample, and finally the average value was calculated.

The grain size of the LSEM-ed chips was measured using the linear intercept method following the ASTM standard E112-13 [13].

Vickers micro-hardness measurements of both the machined bar and LSEM-ed chips were carried out using a Leitz Durimet™ micro-hardness tester with a load of 98 mN for 30 s; three values were recorded for each measurement and then the average calculated. In the case of the machined bar, measurements were taken every 20 µm from the machined surface till a depth of 200 µm. Whereas for the LSEM-ed chips, the measurements were taken along the section (at the opposite extremities and at the center).

3.4 Corrosion behavior

The corrosion performances of the machined bar and LSEM-ed chips were studied using the same procedure. A standard three electrodes cell, where the AZ61 samples were the working electrode, a Saturated Calomel Electrode (SCE) the reference electrode, and a platinum electrode the counter electrode was used. An Amel^{TM} 2549 potentiostat was used for the electrochemical tests. The potentiodynamic polarisation curves were obtained applying a potential from -2.5 V to 0.5 V at a scan rate of 0.5 mVs^{-1}, in Simulated Body Fluid (SBF) solution and at body temperature (37± 1°C) [14]. The corrosion potential *Ecorr* and corrosion current density *Icorr* were determined from the polarization measurements using the Tafel extrapolation method, according to the ASTM G5-14 standard [15]. The electrochemical tests were repeated three times in order to assure the results reproducibility.

4. Results and discussion

4.1. Chip morphology

Fig. 2 shows pieces of chips obtained under the cutting conditions of Table 1. The LSEM process was able to suppress the chip segmentation, exploiting the combination of pressure and heat arisen from the plastic work. In fact, it is worth noting that the obtained chips were always continuous, except for the C1 case in which fractures at regular intervals of 50 mm were found. This can be attributed to the low cutting speed, and, therefore, higher cutting time compared to the other cases, during which the temperature was kept very low by the constant liquid nitrogen adduction, which contributed to reduce the material plasticity. On the other hand, as regards the D1 case, the temperature was high enough to form continuous chips, but not enough to avoid the presence of cracks along the chip section.

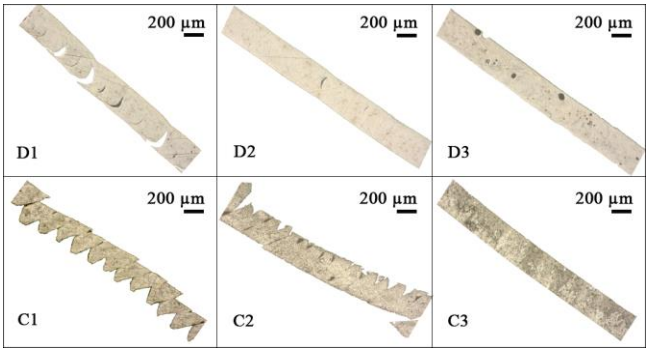

Figure 2. Chips obtained under the cutting conditions of Table 1.

In the C2 case, the temperature rises due to cutting promoted a sensible reduction of the shear bands, even though they were still present. On the contrary, the chip obtained under D2 conditions was perfectly continuous and defect-free. At the highest cutting speed, the increase of shear strain rate induced a localized heat generation in the deformation zone, which enhanced the material plasticity and helped avoiding shear banding of the chips; therefore, even in cryogenic conditions, the chips were found continuous and defects-free.

4.2. Microstructure and mechanical characterization of the machined bars

Fig. 3 a) and b) shows two different microstructures of the bar obtained under dry and cryogenic cooling conditions at the same cutting speed.

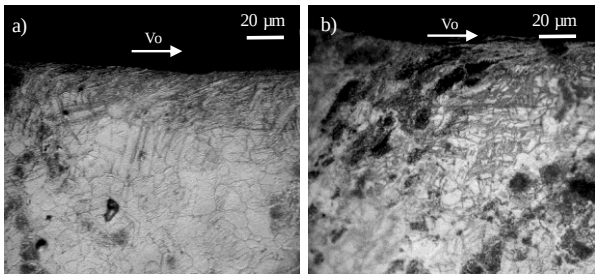

Figure 3. Microstructures of the machined bar: (a) D3 case, and (b) C3 case.

In general, a SPD region near the machined surface, formed by heavily deformed grains, which are strained and elongated along the cutting speed direction, can be found regardless of the cutting conditions. This SPD region presents very fine grains, drastically reduced in size compared to the ones of the initial annealed structure. Below this region, the grain size gradually returns to the value of the annealed microstructure. Table 2 reports the thickness of the UFG region as a function of the cutting conditions of Table 1.

Table 2. Thickness of the SPD region as a function of the cutting conditions of Table 1.

Test ID	UFG region thickness (µm)
D1	27.7 ± 4
D2	30.7 ± 4
D3	33.9 ± 6
C1	26.5 ± 2
C2	32.8 ± 2
C3	45 ± 4

The use of cryogenic cooling favored grain refinement (see Fig. 3b) and a slightly increase of the thickness of the UFG region compared to the dry cases, especially when the highest cutting speed was adopted. This peculiar behaviour in cryogenic LSEMed samples can be attributed to the large plastic deformation induced by constrained machining together with the suppression of heat due to the spraying of liquid nitrogen during the process itself.

It is worth noting that also the cutting speed influenced the thickness of the UFG region: the change of the cutting speed from 30 m/min to 120 m/min significantly increased the thickness of the affected layer.

Fig. 4 shows the micro-hardness variation from the LSEMed

surface to the substrate of the workpiece as a function of the cutting parameters. A severe hardening that extends up to several tens of microns beneath the surface is present in all the investigated conditions, reflecting the formation of a SPD microstructure (see Fig. 3).

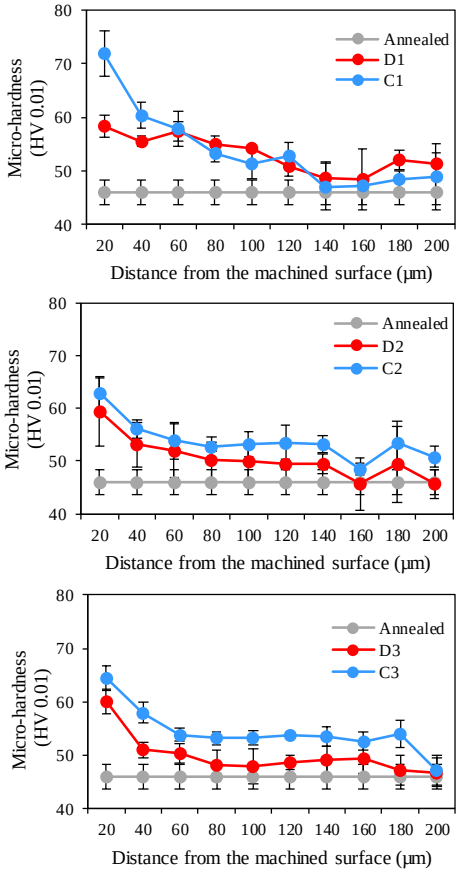

Figure 4. Micro-hardness of the machined bars as a function of the cutting conditions of Table 1.

In general, cryogenic machined samples present higher micro-hardness than the dry cut ones, especially at the lowest investigated cutting speed. In particular, the C1 case presents the highest micro-hardness among all the conditions, reaching an increase up to 64% compared to the base alloy. This can be ascribed to the fact that cryogenic machining contributed to reduce the cutting temperatures and promoted a hardness increment due to the combination of reduced thermal softening and greater grain refinement [16].

The effect of cutting speed reflects that found for the microstructures: harder surfaces are found at higher distances from the machined surface.

The effect of the shear strain rate, which is directly correlated with the cutting speed, on the hardness was not as expected, as it decreased at increasing strain rate. This can be attributed to the prevalent effect of the temperature on the strain hardening as a consequence of the adoption of higher shear rate. It is worth noticing that no sensible differences were found for those samples machined at higher cutting speed; this can be attributable to the presence of a threshold above which the material becomes no sensible any more to the strain rate increase [8]. Moreover, the temperature is supposed to increase monotonically with the cutting speed, but at high speed it was demonstrated that it reached a constant saturation value [17].

4.3. Microstructural and mechanical characterization of the LSEM-ed chips

Fig. 5 shows optical micrographs of typical LSEM-ed chip microstructures, while Table 3 reports their average grain size. Chips of the D2 and D3 cases (Fig. 5a) show an equiaxed and defects-free microstructure indicative of the occurrence of dynamic recrystallization [17]. The average grain size of the D2 case chips is 3 µm, meaning a five times refinement of the grain size with respect to the one of the base alloy after the annealing treatment. A similar equiaxed microstructure was observed in the D3 case: doubling the cutting speed from 60 m/min to 120 m/min did not provide any evident microstructural change in terms of grain growth. This can be attributable to the achievement of a saturation value for the cutting speed, above which the temperature, which is the main driving force to the grain growth, does not increase anymore proportionally with the cutting speed [17]. To be noticed that the relatively low standard deviations in Table 3 are a sign of very homogeneous microstructures.

On the contrary, the LSEM-ed chips obtained in cryogenic conditions together with the D1 case chips show a microstructure similar to the one in Fig. 5b) for the C3 case, which reflects a cold-worked type microstructure, confirmed by the presence of twins within the grains and microstructural features that cannot be resolved through optical microscopy. Table 3 shows also that the resulting grain sizes are higher compared to the D2 and D3 cases. As regards the cryogenic cases, regardless of the cutting speed, this can be attributable, to the application of liquid nitrogen, whereas, in D1 case, to the relatively low cutting speed; in both conditions, the temperature remains always below 200°C, namely the threshold value necessary to start recrystallization phenomena in magnesium alloys [18].

Fig. 6 shows the micro-hardness values of the LSEM-ed chips as a function of the cutting parameters. In general, the abduction of liquid nitrogen leads to a micro-hardness increase. In particular, the C1 case chip presents the highest micro-hardness, with an increase of more than 90% compared to the base alloy, reflecting what happened to the machined bar (see §4.2). This behavior can be explained by the fact that cold-worked microstructures preserve dislocations and twins that both contribute to increase hardness, as a result of the lowest process temperature kept for the longest time. Within dry cases, D1 chips present the highest micro-hardness due to the preservation of a cold-worked microstructure. The strength decrease found in the D2 and D3 cases is compatible with recrystallized microstructures, where dislocations are annihilated due to the nucleation of new grains [10].

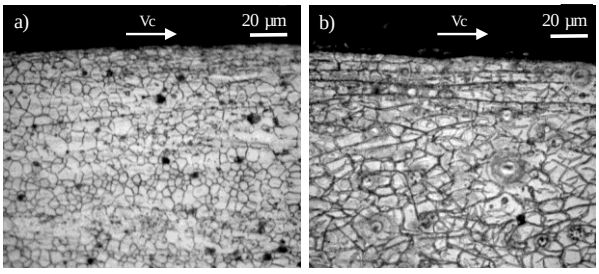

Figure 5. Microstructures of the LSEMed chips: (a) D3 case, and (b) C3 case.

Table 3. Average grain size of the obtained chips.

Test ID	Average grain size (µm)
Annealed	15 ± 4
D1	9.6 ± 4
D2	3.0 ± 2
D3	3.0 ± 1.8
C1	9.8 ± 5
C2	10.6 ± 4
C3	10.0 ± 6

Moreover, the chips of the D2 and D3 cases show almost no differences in micro-hardness, as they have approximately the same grain size. Anyway, the micro-hardness results higher than the one of the base alloy, regardless of the cutting conditions, as a result of the Hall-Petch's effect.

Fig. 6 also shows that hardness varies marginally along the LSEM-ed chips sections. In the case of chips produced under cryogenic cooling, this means that the application of the liquid nitrogen does not lead to any temperature gradient along the chip section.

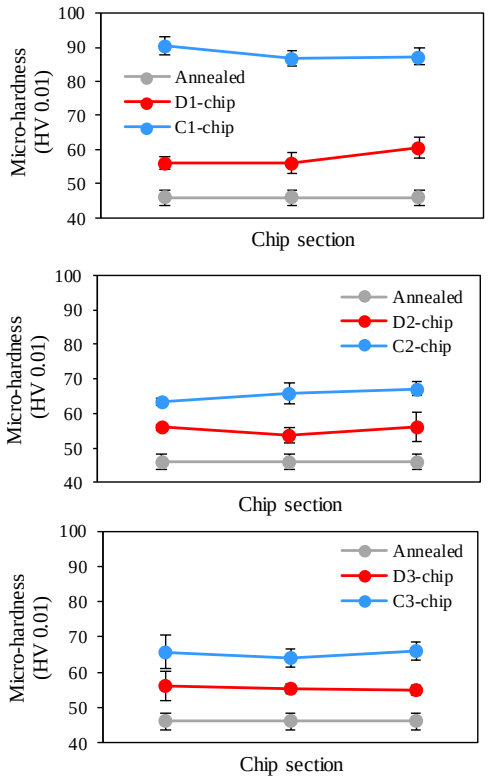

Figure 6. Micro-hardness of the LSEMed chips as a function of the cutting conditions of Table 1.

4.4. Corrosion behavior of the machined bars

Fig. 7 a) reports the potentiodynamic polarization curves of the D2 and C2 cases as well as the one of the base alloy in annealed conditions. Very similar corrosion curves were obtained for the other cutting conditions, and therefore, not here reported. Fig. 7 b) reports the electrochemical data derived from the potentiodynamic polarization curves for all the investigated conditions. In general, an improvement of the corrosion performances can be found compared to the annealed condition as the curves are all shifted towards higher potentials and lower corrosion densities.

Cryogenic cooling led to a slight improvement of the corrosion resistance, and in particular to a very different trend of the anodic branch of the curve. As a matter of fact, in case of the dry LSEMed samples, at a potential equal to 0.65 V, the corrosion curve presents a plateau. This is a sign of an increase of the corrosion tendency, as the corrosion current presents a sudden increase, reaching an extremely high value comparable to that of the annealed condition. The corrosion current has in fact a direct relationship with the corrosion rate: this means that an increase of *Icorr* corresponds to an increase of the mass lost by the implant during its service-life in the human body. As regards the cutting speed, also in this case a clear influence cannot be identified.

After LSEM, the machined bar grain size decreased in a sensible way compared to the initial one, as shown in Fig. 3. Previous studies [19, 20] reported that finer grains could enhance the corrosion properties of magnesium alloys. Finer grains are usually associated with the formation of a strengthened passive film [21]. The presence of a plateau in the corrosion curves relevant to dry cutting can be attributed to a breakdown of the material surface oxide. The higher refinement provided by cryogenic conditions gave enough strength to the surface oxide to avoid its rupture.

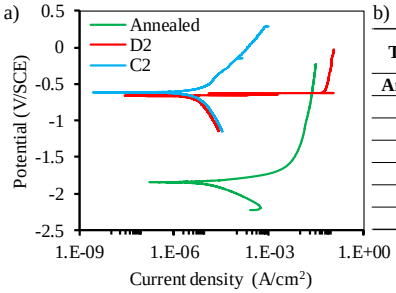

Test ID	Ecorr (V/SCE)	Icorr (µA/cm²)
Annealed	-1.84	10
D1	-0.72	7
D2	-0.66	6
D3	-0.58	10
C1	-0.69	9
C2	-0.62	2
C3	-0.59	2

Figure 7. a) Potentiodynamic polarisation curves in SBF solution at 37°C of the bars machined under D2 and C2 conditions; b) electrochemical corrosion data of the machined bars.

4.5. Corrosion behavior of the LSEM-ed chips

Fig. 8 a) reports the potentiodynamic polarization curves of the chips obtained under D3 and C3 cutting conditions as well as the one of the base alloy in annealed condition, while Fig. 8 b) reports the electrochemical data derived from the curves. It is worth to underline that only the LSEM-ed chips with the best surface quality for each cooling condition were tested for corrosion, namely the D3 and C3 cases, since the presence of cracks drastically increases the surface exposed to the aggressive environment, therefore altering the corrosion curves. Both the curves relevant to chips machined under dry and cryogenic conditions are shifted towards higher potential compared to the base alloy. The D3 case shows a corrosion current that is halved compared to the one of the base alloy, whereas the cryogenic chip shows an increase of a half. The improvement of the corrosion performances in the D3 case chip can be attributed to its grain refinement, since the grain boundaries act as a physical corrosion barrier [22]. C3 LSEM-ed chips present coarser grains than the D2 case chips, but finer

than the base alloy, and, unexpectedly, they are characterized by higher corrosion current than the latter. This can be attributable to the presence of dislocation features characteristic of cold-worked microstructure, which accelerate the anodic metal dissolution, as a consequence of a local reduction of equilibrium potential in the vicinity of dislocations [23].

a)

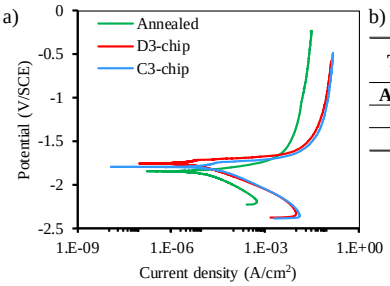

b)

Test ID	Ecorr (V/SCE)	Icorr (μA/cm²)
Annealed	-1.84	10
D3	-1.82	5
C3	-1.8	15

Figure 8. a) Potentiodynamic polarisation curves in SBF solution at 37°C of the chips obtained when machining under D3 and C3 conditions; b) electrochemical corrosion data of the chips.

5. Conclusions

In this study, LSEM was used to induce surface modifications on AZ61 magnesium alloy workpieces. Different cooling strategies and cutting speeds were applied and their effects on the surface integrity and corrosion resistance were evaluated. The main findings can be summarized as follows:

- The strategy of applying liquid nitrogen showed potentialities to obtain a machined surface with enhanced mechanical and corrosion characteristics. In fact, the cryogenic-machined surfaces were characterized by a greater grain refinement and slightly more extended SPD layer compared to the corresponding dry ones. In addition, harder surfaces were observed when liquid nitrogen was applied. Also the corrosion properties were positively influenced, as the characteristic plateau of the corresponding dry curves, indicative of a lower corrosion resistance, was not detected. On the contrary, the main effect of the cutting speed, regardless of the cooling strategy, is limited to the formation of a thicker UFG region on the subsurface of LSEMed samples at increasing cutting speed.

- In general, hard chips characterized by a cold-worked microstructure are obtained when machining with liquid nitrogen, which can be the cause of the defects they present, as a consequence of the overall reduction of the process temperature, especially when low cutting speeds are set. On the contrary, the adoption of dry cutting and higher cutting speeds favors the formation of softer and completely recrystallized chips. Corrosion results indicate that LSEMed chips obtained under dry conditions are characterized by a reduced corrosion current with the respect to the annealed condition. On-going works are focused on the optimization of chips production (thanks to a proper combination of α and λ), even under cryogenic cooling, in order to evaluate their applicability to the manufacturing of sheet-based biomedical devices.

Acknowledgements

The authors wish to thank Mr. Marco Bellin (University of Padova, Italy) for carrying out the machining experimental campaign.

References

[1] Peron M, Torgersen J, Berto F, Mg and Its Alloys for Biomedical Applications. Mechanical Failure 2017;7:252.
[2] Zheng YF, Gu XN, Witte F, Biodegradable metals. Mat Sci Eng R 2014;77:1–34.
[3] Ratna Sunil B, Sampath Kumar TS, Chakkingal U, Nandakumar V, Doble M, Devi Prasad V, Raghunath M, In vitro and in vivo studies of biodegradable fine grained AZ31 magnesium alloy produced by equal channel angular pressing. Mater Sci Eng C 2016;59:356–367.
[4] Denkena B, Lucas A, Biocompatible magnesium alloys as absorbable implant materials adjusted surface and subsurface properties by machining processes. CIRP Manuf Technol 2007;56:113–6.
[5] Zhang CZ, Zhu SJ, Wang LG, Guo RM, Yue GC, Guan SK, Microstructures and degradation mechanism in simulated body fluid of biomedical Mg–Zn –Ca alloy processed by high pressure torsion. Mat Design 2016;96:54–62.
[6] Saldana C, Yang P, Mann JB, Moscoso W, Gill DD, Chandrasekar S, Trumble KP, Micro-scale components from high-strength nanostructured alloys. Mat Sci Eng A 2009;503:172–5.
[7] Moscoso W, Bulk nanostructured materials by large strain extrusion machining. J Mat Research 2007;201–5.
[8] Cai J, Shekhar S, Wang J, Shankar MR, Nanotwinned microstructures from low stacking fault energy brass by high-rate severe plastic deformation. Scr Mater 2009;60:599–602.
[9] Jawahir IS, Puleo DA, Schoop J, Cryogenic machining of biomedical implant materials for improved functional performance, life and sustainability. Procedia CIRP 2016;46:7–14.
[10] Lafayette W, Kustas AB, Compton WD, Direct Single-Stage Processing of Lightweight Alloys Into Sheet by Hybrid Cutting – Extrusion. J Manuf Sci Eng 2017;137:1–10.
[11] A. Bordin A, S. Bruschi S, A. Ghiotti A, P.F. Bariani PF, Analysis of tool wear in cryogenic machining of additive manufactured Ti6Al4V alloy. Wear 2015;328–9:89–99.
[12] Deng WJ, Lin P, Li Q, Xia W, Effect of Constraining Tool Corner Radius on Large Strain Extrusion Machining. Mat Manuf Processes 2013;2:1090–4.
[13] ASTM E 112-13 Standard Test Methods for Determining Average Grain Size. West Conshohocken, PA United States.
[14] Bertolini R, Bruschi S, Ghiotti A, Pezzato L, Dabalà M, The effect of cooling strategies and machining feed rate on the corrosion behavior and wettability of AZ31 alloy for biomedical applications. Procedia CIRP 2017;65:7–12.
[15] ASTM G5-14 Standard Reference Test Method for Making Potentiodynamic Anodic Polarization Measurements. West Conshohocken, PA United States.
[16] Yang S, Dillon OW, Puleo DA, Jawahir IS, Effect of cryogenic burnishing on surface integrity modifications of Co-Cr-Mo biomedical alloy, J Biomed Mater Res. - Part B 2013;101:139–152.
[17] Efe M, Moscoso W, Trumble KP, Compton WD, Mechanics of large strain extrusion machining and application to deformation processing of magnesium alloys. Acta Mater 2012;60:2031–2042.
[18] Sagapuram D, Efe M, Moscoso W, Chandrasekar S, Trumble KP, Deformation temperature effects on microstructure and texture evolution in high stran rate extrusion-machining of Mg-AZ31B. Mat Sci Forum 2012;702-703-52-5.
[19] Alvarez-Lopez M, Pereda MD, Del Valle JA, Fernandez-Lorenzo M, Garcia-Alonso MC, Ruano OA, Escudero ML, Corrosion behaviour of AZ31 magnesium alloy with different grain sizes in simulated biological fluids, Acta Biomater 2010;6:1763–1771.
[20] Ralston KD, Birbilis N, Effect of grain size on corrosion, Corrosion 2010;66:1–4.
[21] Sunday C, Tolouei R, Mostavan A, Paternoster C, Turgeon S, Effect of grain sizes on mechanical properties and biodegradation behavior of pure iron for cardiovascular stent application, Biomatter 2016;6:1–9.
[22] Aung NN, Zhou W, Effect of grain size and twins on corrosion behaviour of AZ31B magnesium alloy, Corros Sci 2010;52: 589–4.
[23] Gutman EM, Legierung E, DC and AC polarisation study on magnesium alloys Influence of the mechanical deformation. Mater Corros 2002;461:455–61.